RSC Advances

PAPER

View Article Online
View Journal | View Issue

Cite this: *RSC Adv.*, 2017, **7**, 46132

A g-C_3N_4/rGO nanocomposite as a highly efficient metal-free photocatalyst for direct C–H arylation under visible light irradiation†

Xiaohui Cai, Hanwen Liu, Lihua Zhi, Huang Wen, Ailing Yu, Lianhua Li, Fengjuan Chen* and Baodui Wang *

Received 6th July 2017
Accepted 13th September 2017

DOI: 10.1039/c7ra07462j

rsc.li/rsc-advances

Visible light mediated photoredox arylations can proceed under very mild conditions and have therefore become attractive. Nowadays, various metal nanomaterials and metal complexes have been developed as photocatalysts for direct arylation of heteroaromatics. These photocatalysts, however, still suffer from corrosion, high cost, aggregation or poor stability. We report the design and fabrication of a g-C_3N_4/rGO nanocomposite and demonstrate its excellent activity, high apparent quantum efficiency, and recyclability to catalyze the metal free direct arylation of heteroaromatics under visible light at room temperature. Moreover, the g-C_3N_4/rGO catalyst can be reused more than five times without significant loss of activity, confirming this catalyst's excellent stability. The present strategy to fabricate a metal-free g-C_3N_4/rGO nanocomposite for direct C–H arylation open a new avenue towards replacing metal-based catalysts in fine organic synthesis.

1. Introduction

Arylated heteroarenes are widely used in materials science due to their interesting optical and electronic properties. Simultaneously, these compounds exhibit remarkable biomedical applications, especially in peptide mimetics or pharmaceuticals.[1–5] The most efficient synthesis of aryl-heteroaryl bonds is the direct C–H arylation of heteroarenes.[6,7] Recently, using visible light driven-metal catalysts for C–H arylation has attracted significant attention.[8–13] Compared with metal-based catalysts, the metal-free photocatalysts undoubtedly provide a valuable strategy to overcome the drawbacks caused by metals. It's well-known that the metal can be compromised, dissolved or decomposed in the reaction system and also cause detrimental environmental pollution problems.[14–17] Very recently, König reported using Eosin Y, a high-cost organic photosensitizer, as a metal-free photocatalyst for direct arylation of heteroarenes.[18] However, the cost, recycling and reuse of the photocatalyst is still a problem. Hence, the development of efficient, low-cost, sustainable, environmentally friendly, metal-free photocatalytic materials for C–H arylation is urgently required.

The graphitic carbon nitride (g-C_3N_4) is a fascinating photocatalyst,[19–22] which absorbs the visible light with a medium band gap (2.4–2.8 eV). Due to the exceptional physicochemical stability, earth-abundant, low-cost, green precursors and especially the metal-free feature, it is a better candidate of photocatalyst. However, the photocatalytic efficiency of bare g-C_3N_4 is limited by the high recombination rate of photogenerated electron–hole pairs. In addition, the weak van der Waals interaction between adjacent conjugated planes also hinders the electron coupling between the planes, which negatively affects the electron transfer and the photocatalytic activity.[23] To resolve this problem, many attempts have been carried out to improve the photocatalytic performance of g-C_3N_4, such as non-metal doping, noble metal deposition, preparation of nano-porous g-C_3N_4 or 2D materials hybriding.[24,25] In fact, introducing 2D graphene or its derivatives can promote the photo-generated charge separation and transfer, resulting to minimize recombination losses, which is an effective strategy to improve visible light utilization, and electron transport property of g-C_3N_4.[26] Recently, the composites of g-C_3N_4 and 2D graphene have been widely used in photocatalytic water splitting, dyes removal and so on.[27,28] Up to now, there has been no report on the use of the g-C_3N_4/rGO nanocomposite as photocatalyst for visible light driven-direct C–H arylation.

Here we developed the g-C_3N_4/rGO nanocomposite by thermally treating the precursor materials consisted of melamine and rGO at 550 °C for 4 h in nitrogen. The precursor of melamine was polymerized to g-C_3N_4. On account of the similar carbon network and sp^2 conjugated π structure, the g-C_3N_4 are very facile compatibility with rGO to form the "sandwich structure". Such unique structure is essential for improving the photo-generated electron transfer and photocatalytic activity of

Key Laboratory of Nonferrous Metal Chemistry and Resources Utilization of Gansu Province, State Key Laboratory of Applied Organic Chemistry, Lanzhou University Gansu, Lanzhou, 730000, P. R. China. E-mail: wangbd@lzu.edu.cn; chenfj@lzu.edu.cn

† Electronic supplementary information (ESI) available: Fig. S1–S9, and Table S1. See DOI: 10.1039/c7ra07462j

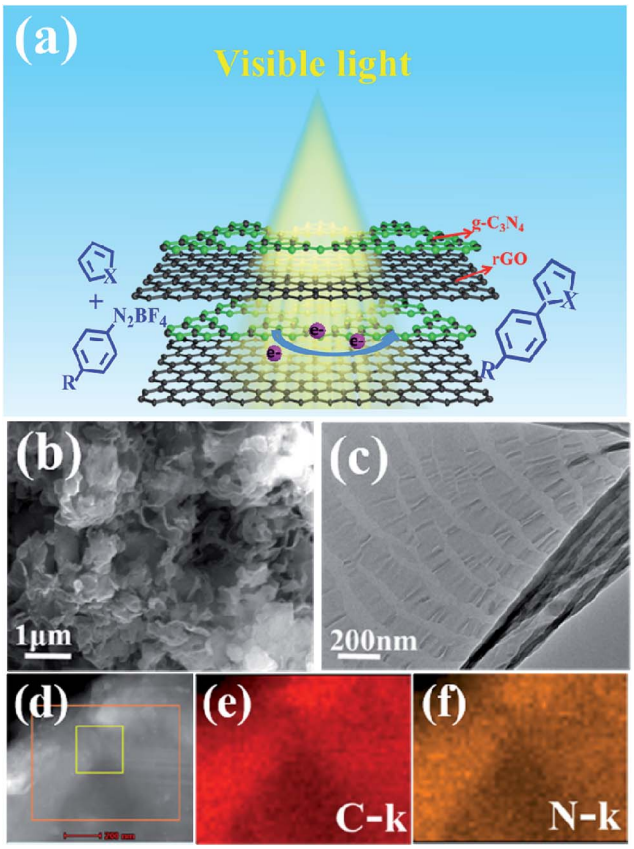

Fig. 1 (a) The schematic illustration of g-C_3N_4/rGO nanocomposite with "sandwich structure" for photocatalysis direct C–H arylation; (b) the SEM image of g-C_3N_4/rGO nanocomposite; (c) the TEM image of g-C_3N_4/rGO nanocomposite; (d) high angle annular dark field scanning TEM images; (e and f) elemental mapping images of g-C_3N_4/rGO nanocomposite.

g-C_3N_4.[29] The resulting g-C_3N_4/rGO nanocomposite shows an excellent photocatalytic performance for direct C–H arylation of heteroarenes with aryl diazonium salts under visible light irradiation (the schematic is shown in Fig. 1a). The quantum efficiency is 70.7% at the wavelength of 450 nm.

2. Experimental section

2.1. Materials

All reagents and solvents were obtained commercially and used without further purification unless otherwise noted. Graphite powder was purchased from Sigma-Aldrich. The dialysis bags (MWCO 8000–14 000 g mol^{-1}) were purchased from Shanghai Med. Thiophene (99%) and furan (98%) were purchased from J&K Scientific Ltd. Hydrogen peroxide, sulphuric acid (95–97%), sodium nitrite, *N*,*N*-dimethyl formamide (DMF), and potassium permanganate were obtained from Tianjin Med. Hydrazine hydrate (85%), and melamine were purchased from Sinopharm Chemical Reagent Co., Ltd.

2.2. Instrumentation

^{1}H NMR spectra and ^{13}C NMR spectra were acquired with Varian 400 MHz NMR. X-ray photoelectron spectroscopy (XPS) measurements were performed on a PHI-5702 multifunctional spectrometer using AlKα radiation. FT-IR spectra were recorded on a Nicolet FT-170SX spectrometer. Photocatalysis was performed using daylight lamp. X-ray diffraction (XRD) patterns were obtained on a Bruker AXS D8 advance diffractometer with CuKα radiation (λ = 1.5418 Å). The transmission electron microscope (TEM) was operated on a JEM-2100 (200 kV) instrument. UV-visible adsorption spectra (UV-vis) were calculated by a UV 1750 spectrometer. The yields were determined by 450-GC gas chromatograph.

2.3. Preparation of GO[30]

Concentrated sulfuric acid (46 mL) in a 250 mL flask was setted in an ice bath with mechanical agitation at 250 rpm. After cooling down the solution to <10 °C, graphite powder (1.0 g, 40 nm, 99%) was added and then $KMnO_4$ (3.0 g) and $NaNO_3$ (3.0 g) were slowly added to the mixture and keep the temperature of the suspension <10 °C. Successively, the reaction system was transferred to a 40 °C oil bath and vigorously stirred for 2 h. Then 100 mL water was slowly added to the reaction system. Subsequently, the reaction mixture was poured into 150 mL water and some H_2O_2 (30%) liquor was added dropwise. At this time, the color of the solution changed from dark brown to yellow. The mixture was centrifuged at 8000 rpm for 2 min and washed with water and NaCl solution to remove metal ions and keep the pH at 6. The resulting solid was dispersed in 200 mL water to form a GO aqueous dispersion. Then the solution was sonicated for 36 h. Finally, it was purified by dialysis for one week using a dialysis bag with a molecular weight cutting off of 8000 to 14 000 g mol^{-1} to remove the remaining acid and metal species.

2.4. Preparation of rGO

The distilled water (150 mL) was added into a flask (250 mL), then the certain volume of GO dispersed in aqueous solution (2 g L^{-1}) was added under ultra sonication for 1 h. GO in the synthesis compounds was reduced by adding hydrazine hydrate (4 mL) under stirring at 90 °C for 24 h. After that, rGO was made, which was collected by centrifugation and was washed three times with methanol and two times with distilled water, and then dried in an oven.

2.5. Preparation of g-C_3N_4/rGO[31]

All chemicals were analytical grade purity and distilled water was used in the whole experiment. g-C_3N_4/rGO nanocomposite was prepared by an impregnation-chemical reduction strategy. The melamine (2.0 g) and reduced graphene oxide (rGO) were put into a crucible (30 mL) with a cover and heated at 550 °C for 4 h and kept at this temperature for another 4 h under flowing nitrogen, subsequently cooled to room temperature. The weight percentages of rGO in the photocatalyst samples were 0, 0.5, 1.0, and 2.0 wt% respectively.

2.6. Preparation of aryldiazonium salts

The aryldiazonium salts were prepared according to the literature with slight modification.[32] The corresponding aniline

(0.02 mol) was dissolved in a mixture of ultrapure water (8 mL) and 50% fluoroboric acid (6.8 mL). After the temperature fell below zero, 3 mL sodium nitrite solution (1.38 g) was added slowly. The mixture was stirred for 40 minutes in ice bath, and the resulting precipitate was collected by centrifuging and washed several times with aether. The resulting solid was recrystallized by acetone and aether.

2.7. The apparent quantum efficiency (AQE) calculation

A 300 W Xe arc lamp was used as the light source for photocatalytic reaction. The measurement of AQE was performed using same amount of reactants. We fixed the wavelength at 400 nm< λ < 700 nm for vis-irradiation. The laser power in the photocatalytic reaction was collected using a power meter (Newport; 843R). The corresponding wavelength captured for AQE calculation is located at 450 nm. Thus the AQE is calculated as the following equation, AQE = $n/n_p \times 100\%$, in which n and n_p are denoted as number of photons that generating product needed and the number of incident photons, respectively. The apparent quantum efficiency (AQE) was calculated. The reaction condition is as follows: 0.1 mmol **1a**, 4 mg g-C_3N_4/rGO nanocomposite, 1 mL DMF, 1 mL furan, under visible light irradiation (450 nm) for 15 min. During the reaction process, total absorb light energy $\Delta E = 18.4–5.1 = 13.3$ J, $N = 0.53 \times 1$ mmol $= 0.53$ mmol, energy per photon $E_0 = hc/\lambda = 6.63 \times 10^{-34} \times 3 \times 10^8/(450 \times 10^{-9}) = 4.42 \times 10^{-19}$ J, molar of photons $n_p = [\Delta E/(E_0 \times N_A)] \times t = [13.3/(4.42 \times 10^{-19} \times 6.02 \times 10^{23})] \times 15 = 0.75$ mmol, AQE (initial) $= n/n_p = 0.53/0.75 \times 100\% = 70.7\%$. With the same method, we can calculate the initial AQE of other catalysts, respectively.

3. Results and discussion

3.1. Preparation and characterization of g-C_3N_4/rGO

The unique "sandwich structure" of g-C_3N_4/rGO nanocomposites are confirmed by scanning electron microscope (SEM) and transmission electron microscopy (TEM). Fig. 1b shows the SEM image of g-C_3N_4/rGO nanocomposite with the rGO content of 1.0 wt% (g-C_3N_4/rGO-1). The result indicates that the morphology of g-C_3N_4/rGO-1 nanocomposite is similar to cotton, which may be attribute to the fact that g-C_3N_4 grows along the two-dimensional nano-sheet of rGO to form fluffy nanocomposite. The TEM image further displays that the g-C_3N_4/rGO nanocomposite exhibits multilayer structures, and the g-C_3N_4 is sandwiched between rGO sheets (Fig. 1c). The elemental mapping images (Fig. 1e and f) detailed shows the presence and homogeneous distribution of C and N elemental in g-C_3N_4/rGO nanocomposite. The SEM and TEM characterization of pure g-C_3N_4, rGO and g-C_3N_4/rGO nanocomposite with different rGO ratios are shown in Fig. S1.†

As shown in Fig. 2a, the X-ray diffraction (XRD) patterns of rGO presents broad signal at 24.2°, which corresponds to the (001) diffraction peak of interlayer spacing.[33] Two distinct diffraction peaks of g-C_3N_4 and g-C_3N_4/rGO-1 nanocomposite are present at 13.1° and 27.5°, which associate with the (100) and (002) reflection indexes of g-C_3N_4 respectively.[34] In Fig. 2b, the XPS survey spectrum revealed the existence of C, N, and O species in –C_3N_4/rGO-1 nanocomposite. As shown in Fig. S3,† comparing with the pure g-C_3N_4 and/rGO, the FTIR spectra of g-C_3N_4/rGO nanocomposite also exhibits the same groups stretching of rGO and pure g-C_3N_4. These results indicate that the g-C_3N_4 and rGO coexist in the g-C_3N_4/rGO nanocomposite.

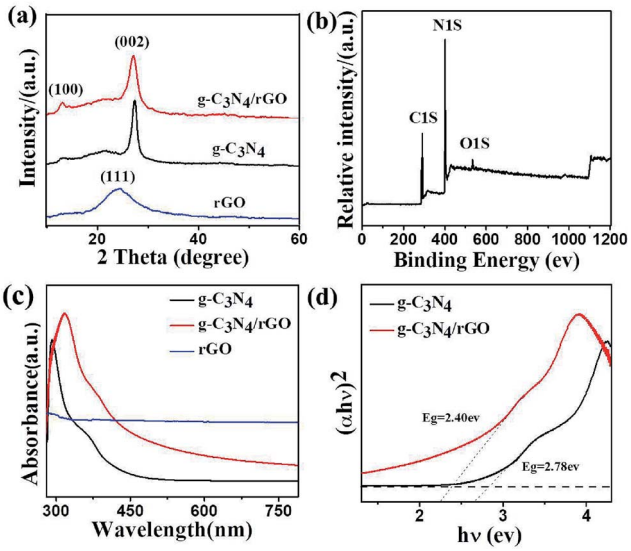

Fig. 2 (a) XRD patterns of pure g-C_3N_4, rGO and g-C_3N_4/rGO nanocomposite; (b) XPS spectra of the g-C_3N_4 and g-C_3N_4/rGO nanocomposite; (c) UV-vis diffuse reflectance spectra of the pure g-C_3N_4, g-C_3N_4/rGO nanocomposites and rGO; (d) the plots of transformed Kubelka–Munk functions *versus* the light energy.

The UV-vis diffuse reflectance spectra of pure g-C_3N_4 and g-C_3N_4/rGO-1 nanocomposite are shown in Fig. 2c. The results illustrate that both of the samples exhibit strong visible light absorption. Obviously, rGO enormously affects the optical property of the g-C_3N_4/rGO nanocomposite. Moreover, with increasing rGO ratio in g-C_3N_4/rGO nanocomposite, a red shift is observed in the absorption band edge (Fig. 2c and S4a†),[36] which means the band gap narrowing of the nanocomposite.[35] We also have tested the band position and redox potential energy values of g-C_3N_4 by electrochemical technique (Fig. S5†). Fig. 2d shows the plots of the transformed Kubelka–Munk function of light energy about the investigated samples. The estimated band gaps are 2.78 and 2.40 eV, corresponding to pure g-C_3N_4, g-C_3N_4/rGO-1, respectively. Fig. S4b† shows that the band gap of g-C_3N_4/rGO composites becomes more and more narrow with increasing rGO ratio. This supports the result of a red shift in the absorption band edge of g-C_3N_4/rGO nanocomposite. Probably, the reactive oxygen functional groups on the rGO surface (*e.g.*, –OH, –COOH) can play a key role of cross-linkers to form C–O–C covalent bonding between rGO and g-C_3N_4 during thermal conversion, which could be the reason for the band gap narrowing and enhancing visible light absorption of the nanocomposites.[37] The narrow band gap is beneficial to photo-generated electrons.[19–22] However, too high rGO ratio in nanocomposite is also disadvantageous because most of the incident light will be absorbed by rGO, resulting in a decreased light utilization of g-C_3N_4.[39] Therefore, an appropriate rGO ratio in nanocomposite could be

critically important for improving the light utilization and photocatalytic efficiency.

Photoluminescence (PL) analysis is performed to investigate the suppression of electrons and holes (e^-/h^+) recombination. As shown in Fig. 3, the emission peak of pure g-C_3N_4 appears at 450 nm, which is due to the band–band PL phenomenon with the energy of light approximately equal to the band-gap energy of g-C_3N_4 (2.78 eV), leading to the n–π* electronic transitions in g-C_3N_4.[38] For the g-C_3N_4/rGO nanocomposite, the modification of rGO causes fluorescence quenching. The degree of fluorescence quenching was obviously increased with the increase of rGO ratio. The result demonstrates that the recombination of photo-generated electrons and holes is greatly inhibited by the introduction of rGO because rGO acting as an electron collector, which indicates that the separation of photogenerated e^-/h^+ in the g-C_3N_4/rGO composites is more efficient than in pristine g-C_3N_4.[39] As a whole, the appropriate rGO ratio can improve light utilization and photocatalytic efficiency.

3.2. Photocatalytic property

Subsequently, we investigate the photocatalytic activity of g-C_3N_4/rGO nanocomposite to direct arylation of diazonium salt (**1a**) with furan (**2a**) under visible light irradiation (λ > 420 nm) at room temperature. Firstly, various solvents are used at room temperature. As shown in Table 1, the reaction in *N*,*N*-dimethylformamide (DMF) could provide the target product in ideal yield of 91% (as shown in Table 1). Fig. 4b presents a comparison of the visible light driven-photocatalytic performance of g-C_3N_4/rGO nanocomposite with different rGO contents (0, 0.5, 1.0, 2.0 wt%) for direct arylation. The result shows that the rGO content has a significant influence on the photocatalytic activity of g-C_3N_4. The pure g-C_3N_4 shows a general photocatalytic activity and the product yield is 66%, owing to the moderate band gap and unique electronic structure of g-C_3N_4. In the presence of a small amount of rGO (0.5 wt%), the activity of the nanocomposite is remarkably enhanced. The photocatalytic activity of the samples further increased with increasing rGO content to 1.0 wt%, and the highest product yield of 91% is obtained. When the rGO content is higher than 1.0 wt%, the photocatalytic activity of the nanocomposite is rapidly decreased. This decline

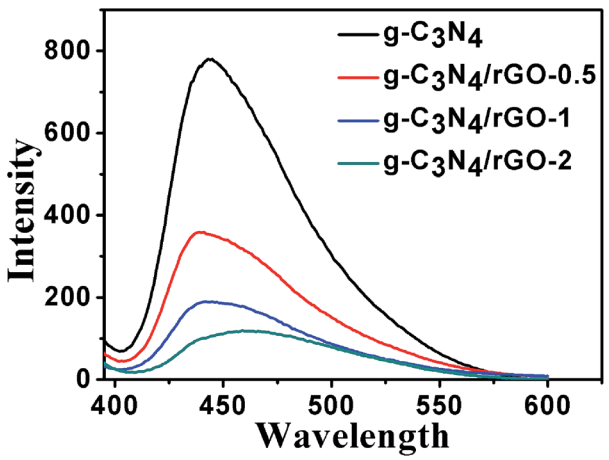

Fig. 3 Photoluminescence (PL) spectra of the g-C_3N_4 and g-C_3N_4/rGO nanocomposites. The extent of the fluorescence quenching was found to be obviously increased with increasing rGO ratio in the g-C_3N_4/rGO nanocomposites.

Table 1 Photoreaction was performed in different solvents. Reaction conditions: 0.1 mmol **1a**, 4 mg g-C_3N_4/rGO nanocomposite, 1 mL solvent, 1 mL furan, irradiation with visible light for 1.5 h under nitrogen atmosphere. All the yields were determined by GC

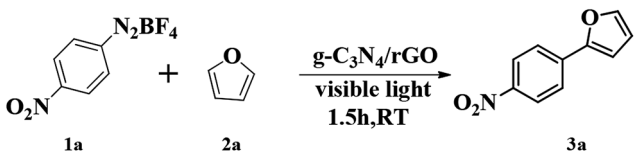

Entry	Reaction condition	Yield [%]
1	DMF	91%
2	EtOH	80%
3	MeOH	68%
4	MeCN	52%
5	Acetone	0%
6	Isopropanol	6%
7	*n*-Hexane	6%
8	1,4-Dioxane	7%

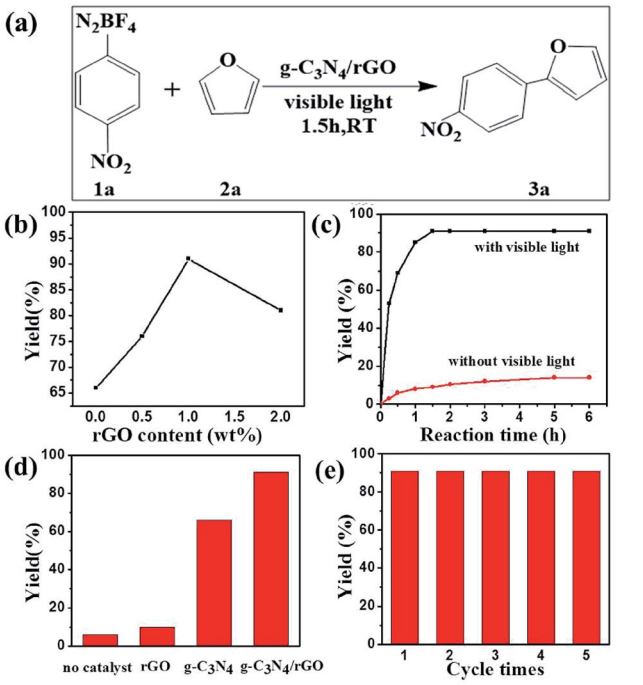

Fig. 4 (a) Reaction condition: 0.1 mmol **1a**, 4 mg g-C_3N_4/rGO nanocomposite, 1 mL DMF, 1 mL furan, under visible light irradiation for 1.5 h in nitrogen atmosphere. All the yields were determined by GC. (b) Effects of rGO content on the photocatalytic performance of g-C_3N_4/rGO nanocomposite; (c) the visible light effect on the photocatalytic activity of g-C_3N_4/rGO nanocomposite; (d) photocatalytic activities of the g-C_3N_4, rGO, and g-C_3N_4/rGO nanocomposite for direct C–H arylation; (e) the reusability of g-C_3N_4/rGO nanocomposite for direct C–H arylation under visible light irradiation.

could be related to the increase in the opacity and light scattering, leading to a decrease of irradiation passing through the reaction suspension solution. The results are similar to the previous studies showing that a suitable loading content of graphene is crucial for optimizing the photocatalytic activity of graphene/g-C_3N_4 and graphene/TiO_2 nanocomposites.[31,39–41] As shown in Fig. S8,† the color of g-C_3N_4/rGO nanocomposite changes from yellow to gray with increasing the ratio of rGO. It can be concluded that the rGO ratio affect the light scattering of the photocatalytic reaction system. In further study, the reaction kinetic of formation of *p*-nitrophenol furan (**3a**) with or without visible light irradiation is investigated. The result illustrates that the yield of the target product is reached 91% under visible light irradiation in a relatively short time of 1.5 h. Meanwhile, there is no by-product formation with the time extension. Otherwise, in the absence of visible light irradiation, the productivity is only 18% after 6 hours reaction (Fig. 4c). The result displays that the photocatalytic direct C–H arylation using g-C_3N_4/rGO-1 nanocomposite could be due to a direct photo-generated electron transfer under visible light irradiation. Comparing with rGO, pure g-C_3N_4 or no catalyst, the g-C_3N_4/rGO nanocomposite as a photocatalyst provides the highest yield of 91% of the target product (Fig. 4d). The result confirms that g-C_3N_4/rGO nanocomposite has an excellent photocatalytic activity for direct C–H arylation. In addition, the stability of g-C_3N_4/rGO nanocomposite is tested. The metal-free catalyst can be separated easily by centrifugation and allowed the repetitive usage without loss of performance at least five times recycles (as shown in Fig. 4e).

Under optimized reaction conditions, we studied the substrate scope of the g-C_3N_4/rGO nanocomposite photocatalytic direct C–H arylation (Table 2). As forming direct C–H arylation of furan with aryldiazonium salts (**1a–f**), various functional groups are tested. Among the aryl diazonium salts used for direct arylation of furan, electron-acceptor-(nitro) and neutral-(halogen) substituted diazonium salts were found more efficient for target product formation than electron-donor-substituted ones (methoxy). The metal-free photocatalyzed C–H arylation was also effective for other heteroarenes, such as thiophene, and the ideal products are obtained in good yields (**4a–d**). We are also compared with other photocatalysts reported of photocatalyzed C–H arylation (Table S1†).

3.3. Mechanism studies

In the previous studies,[18,42] single-electron transfer (SET) mechanism was proposed for photocatalytic C–H arylation. In this work, in order to verify that such single-electron comes from the g-C_3N_4/rGO photocatalyst, 1,4-benzoquinone (BQ) is added to trap the electrons, the photocatalytic activity obviously decrease compared with the reaction without BQ (as shown in Fig. S6†), indicating that the photogenerated electron plays a key role in the photocatalytic reaction. Meanwhile, the *N*,*N*-diisopropylethylamine (DEIA) as a hole scavenger is added, which has no effect for the product yield (as shown in Fig. S6†). The result further confirms that the electron transfer is the major active species for photocatalytic reaction. As shown in Fig. 5, the photogenerated electrons transfer to aryl diazonium

Table 2 Substrate scope of aryldiazonium salts[a]

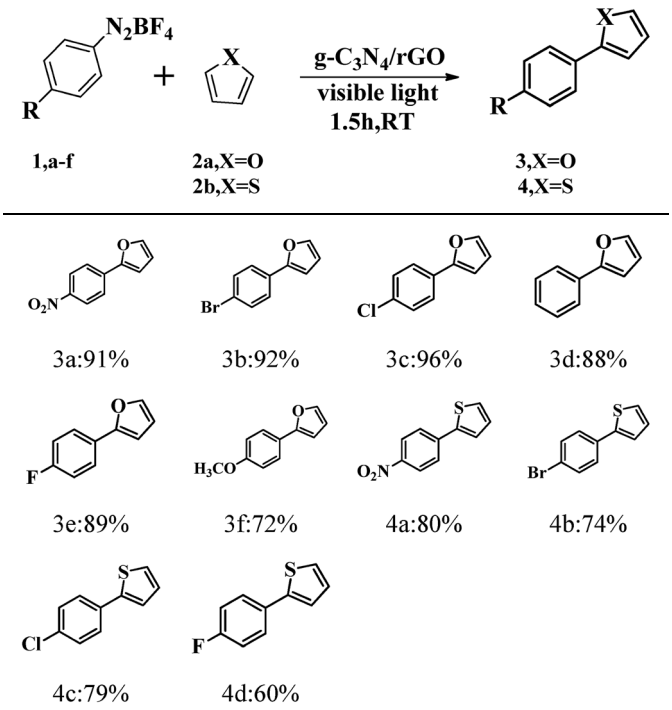

[a] Reaction conditions: 0.1 mmol **1a–f**, 4 mg g-C_3N_4/rGO-1 nanocomposite, 1 mL DMF, 1 mL heteroarene, irradiation with visible light for 1.5 h under nitrogen atmosphere. All the yields were determined by GC.

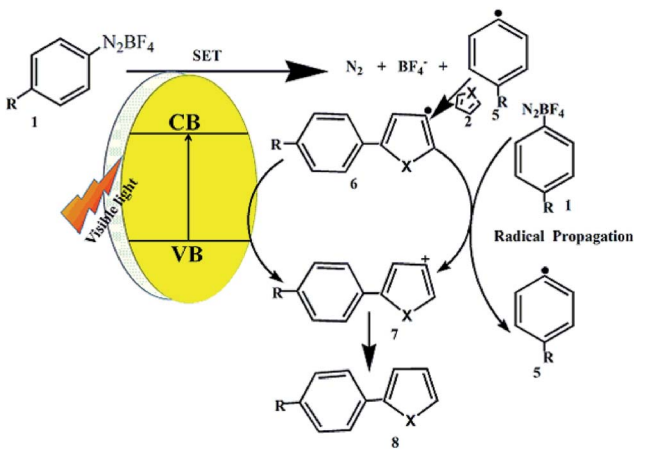

Fig. 5 The proposed reaction mechanism for the g-C_3N_4/rGO nanocomposites direct arylation of heteroarenes.

salt **1** to produce aryl radical **5**. Addition of aryl radical **5** to heteroarene **2** gives radical intermediate **6**, which is further transformed to carbocation intermediate **7** by two possible pathways: (a) oxidation of the radical intermediate **6** by the g-C_3N_4/rGO radical cation to give **7** and (b) the oxidation of **6** by aryl diazonium salt **1** in a radical chain transfer mechanism. Finally, intermediate **7** is protonated, regenerating the aromatic system and leading to the desired coupling product **8**. The

above SET process was further confirmed by the low target product yield when the 2,2,6,6-tetramethylpiperidinoxyl (TEMPO) was added to the above reaction system (as shown in Fig. S7†).[18]

4. Conclusions

In summary, a sandwich structure g-C_3N_4/rGO nanocomposite has been designed. For the first time, such nanocomposite was successfully used as metal-free visible light-driven photocatalyst for direct C–H arylation. The reaction displays an excellent tolerance of substituents with diverse functional groups. The outstanding features of the catalyst are the stability, recyclability, environmentally friendly and low cost. Further applications based on the development of g-C_3N_4/rGO nanocomposite mediated reactions with visible light are the subject of current investigations. The findings of our study provide clear evidence that metal-free g-C_3N_4/rGO nanocomposite has great potential for highly efficient photocatalytic activity for direct C–H arylation, which open a new avenue towards replacing metal-based catalyst in fine organic synthesis.

Conflicts of interest

There are no conflicts to declare.

Acknowledgements

The work was supported by the National Natural Science Foundation of China (21401091, 21671088, and 21431002) and the Fundamental Research Funds for the Central Universities (lzujbky-2017-105).

Notes and references

1 J. G. Mei, K. R. Graham, R. Stalder and J. R. Reynolds, *Org. Lett.*, 2010, **12**, 660–663.
2 H. L. Dong, C. L. Wang and W. P. Hu, *Chem. Commun.*, 2010, **46**, 5211–5222.
3 H. Yin, H. S. Park, G. A. Payne, J. M. Rodriguez, S. M. Sebti and A. D. Hamilton, *Angew. Chem., Int. Ed.*, 2005, **44**, 2704–2707.
4 O. Kutzki, H. S. Park, J. T. Ernst, B. P. Orner, H. Yin and A. D. Hamilton, *J. Am. Chem. Soc.*, 2002, **124**, 11838–11839.
5 M. M. Conn and J. J. Rebek, *Chem. Rev.*, 1997, **97**, 1647–1668.
6 J. O. Trent, G. R. Clark, A. Kumar, W. D. Wilson, D. W. Boykin, J. E. Hall, R. R. Tidwell, B. L. Blagburn and S. J. Neidle, *Med. Chem.*, 1996, **39**, 4554.
7 Y. I. Gorak, N. D. Obushak, V. S. Matiichuk and R. Z. Lytvyn, *Russ. J. Org. Chem.*, 2009, **45**, 541.
8 T. P. Yoon, M. A. Ischay and J. Du, *Nat. Chem.*, 2010, **2**, 527–532.
9 F. Teply, *Collect. Czech. Chem. Commun.*, 2011, **76**, 859–917.
10 L. Shi and W. J. Xia, *Chem. Soc. Rev.*, 2012, **41**, 7687–7697.
11 C. K. Prier and D. A. Rankic, *Chem. Rev.*, 2013, **113**, 5322–5363.
12 N. Hoffmann, *ChemSusChem*, 2012, **5**, 352–371.
13 D. Ravelli, M. Fagnoni and A. Albini, *Chem. Soc. Rev.*, 2013, **42**, 97–113.
14 H. Meerwein, E. Buckner and K. V. Emster, *J. Prakt. Chem.*, 1939, **152**, 237–266.
15 A. Wetzel, V. Ehrhardt and M. R. Heinrich, *Angew. Chem., Int. Ed.*, 2008, **47**, 9130–9133.
16 D. Kalyani, K. B. McMurtrey, S. R. Neufeldt and M. S. Sanford, *J. Am. Chem. Soc.*, 2011, **133**, 18566–18569.
17 P. Tang, G. Hu, M. Z. Li and D. Ma, *ACS Catal.*, 2016, **6**, 6948–6958.
18 P. H. Durga, S. Peter and B. König, *J. Am. Chem. Soc.*, 2012, **134**, 2958–2961.
19 Y. Wang, X. Wang and M. Antonietti, *Angew. Chem., Int. Ed.*, 2012, **51**, 68–69.
20 Y. Chen, J. Zhang, M. Zhang and X. Wang, *Chem. Sci.*, 2013, **4**, 3244–3248.
21 J. Zhu, S. A. C. Carabineiro, D. Shan, J. L. Faria, Y. Zhu and J. L. Figueiredo, *J. Catal.*, 2010, **274**, 207.
22 J. J. Zhu, P. Xiao, H. L. Li and S. A. C. Carabineiro, *ACS Appl. Mater. Interfaces*, 2014, **6**, 16449–16465.
23 C. Zhu, T. Y. J. Han, E. B. Duoss, A. M. Golobic, J. D. Kuntz, C. M. Spadaccini and M. A. Worsley, *Nat. Commun.*, 2015, **6**, 6962.
24 X. C. Wang, X. F. Chen, A. Thomas, X. Z. Fu and M. Antonietti, *Adv. Mater.*, 2009, **21**, 1609–1612.
25 Y. Di, X. C. Wang, A. Thomas and M. Antonietti, *ChemCatChem*, 2010, **2**, 834–838.
26 S. Park and R. S. Ruoff, *Nat. Nanotechnol.*, 2009, **4**, 217–224.
27 Y. Q. Sun, C. Li, Y. X. Xu, H. Bai, Z. Y. Yao and G. Q. Shi, *Chem. Commun.*, 2010, **46**, 4740–4742.
28 G. Z. Liao, S. Chen, X. Quan, H. H. Yu and H. M. Zhao, *J. Mater. Chem.*, 2012, **22**, 2721–2726.
29 X. Cao, J. J. Shi, M. Zhang, X. H Jiang, H. X. Zhong, P. Huang, Y. M. Ding and M. Wu, *J. Phys. Chem. C*, 2016, **120**, 11299–11305.
30 J. Chen, Y. Zhang, M. Zhang, B. W. Yao, Y. R. Li, L. Huang, C. Li and G. Q. Shi, *Chem. Sci.*, 2016, **7**, 1874–1881.
31 Q. J. Xiang, J. G. Yu and M. Jaroniec, *J. Phys. Chem. C*, 2011, **115**, 7355–7363.
32 P. Hanson, J. R. Jones, A. B. Taylor, P. H. Walton and A. W. Timms, *J. Chem. Soc., Perkin Trans. 2*, 2002, 1135–1150.
33 K. Zhang, L. L. Zhang, X. S. Zhao and J. Wu, *Chem. Mater.*, 2010, **22**, 1392–1401.
34 F. Dong, L. Wu, Y. Sun, M. Fu, Z. Wu and S. C. Lee, *J. Mater. Chem.*, 2011, **21**, 15171–15174.
35 J. S. Lee, K. H. You and C. B. Park, *Adv. Mater.*, 2012, **24**, 1084–1088.
36 H. M. Zhang, X. L. Liu, Y. B. Li, Q. F. Sun, Y. Wang, B. J. Wood, P. R. Liu, D. J. Yang and H. J. Zhao, *J. Mater. Chem.*, 2012, **22**, 2465–2472.
37 T. Afroze and A. H. Bhuiyan, *Thin Solid Films*, 2011, **519**, 1825.
38 (*a*) Y. b. Li, H. M. Zhang, P. R. Liu, D. Wang, Y. Li and H. J. Zhao, *Small*, 2013, **9**, 3336–3344; (*b*) V. N. Khabashesku, J. L. Zimmerman and J. L. Margrave, *Chem. Mater.*, 2000, **12**, 3264–3270.

39 G. Z. Liao, S. Chen, X. Quan, H. T. Yu and H. M. Zhao, *J. Mater. Chem.*, 2012, **22**, 2721–2726.
40 J. G. Yu, J. Zhang and M. Jaroniec, *Green Chem.*, 2010, **12**, 1611–1614.
41 J. G. Yu, Y. Hai and B. J. Cheng, *J. Phys. Chem. C*, 2011, **115**, 4953–4958.
42 H. J. Liu, W. Feng, C. W. Kee, Y. J. Zhao, D. S. Leow, Y. H. Pan and C. H. Tan, *Green Chem.*, 2010, **12**, 953–956.